Bio-inspired flapping wing design via a multi-objective optimization approach based on variable periodic Voronoi tessellation

Zeyang Li [a], Kang Gao [a,b], Zhangming Wu [a],*

[a] *School of Engineering, Cardiff University, Newport Rd, Cardiff, CF24 3AA, Wales, UK*
[b] *Key Laboratory of Concrete and Prestressed Concrete Structures of the Ministry of Education, School of Civil Engineering, Southeast University, Nanjing, China*

ARTICLE INFO

ABSTRACT

This paper introduces a novel bio-inspired design methodology for flapping wings in Micro Air Vehicles aiming for achieving optimal physical properties and enhanced aerodynamic performance. The wing's truss structures are derived through a specialized non-periodic, meso-micro scale porous structure optimization technique, termed the "Variable-Periodic Voronoi Tessellation (VPVT)" method. By incorporating critical physical properties such as compliance, natural frequency, and mass transfer efficiency, the VPVT method transforms the complex design metrics into a standard multi-objective optimization process. This approach produces a biomimetic wing design with high geometric fidelity to insect wings. The optimized VPVT design demonstrates notable physical performance improvements over natural wing samples, resulting in a 19.6% increase in stiffness, a 12.5% rise in natural frequency, and a 5.2% enhancement in mass transfer efficiency. Later, the aerodynamic performance is further evaluated via fluid–structure coupling finite element (FE) simulations. Compared to conventional commercial design, the VPVT wing exhibits optimally-tailored local stiffness, resulting in improved aeroelastic behavior during gliding action. Specifically, the FE simulations demonstrate a 7.3% reduction in drag at low angles of attack and a 9.9% increase in lift at high angles of attack. These results indicate the high energy efficiency and maneuverability of the proposed design approach, which enables the design of micro aerial vehicles (MAVs) with long duration and complex maneuverability.

1. Introduction

Flapping flight is the most prevalent mechanism among flying creatures in nature, as aerodynamic and bionic studies have shown that flapping motion is the most suitable form of flight under conditions of low Reynolds number and small wingspan [1]. For instance, the dragonfly can integrate lifting, hovering, and propulsion functions with only two pairs of flapping wings, exhibiting exceptional flight maneuverability and flexibility. Specifically, the wing weight of a dragonfly is less than 5% of its body weight. The dragonfly can achieve a maximum flight speed of approximately 36 km/h, with an average lift coefficient of 2∼3 and an average thrust coefficient of 1∼2 [2]. In comparison, human-designed flapping wings have yet to achieve comparable aerodynamic capability and energy efficiency. Consequently, investigating the relationship between the structure and mechanical behavior of dragonfly wings holds significant scientific value, providing a theoretical foundation and inspiration for the development of Micro Air Vehicles (MAVs) [3–6]. Such studies have the potential to revolutionize the design of air vehicles in environmental monitoring, field rescue, logistical transport, and other applications.

The dragonfly wing's sophisticated and ingenious structure results in anisotropic mechanical properties and distinct biological functionalities. Dragonfly wings consist of an ultra-thin membrane supported by tubular veins, categorized into longitudinal and cross veins [7,8]. Longitudinal veins, which extend along the wingspan, serve as the primary load-bearing elements, further classified into convex veins on the upper wing surface and concave veins on the lower surface. Cross veins connect adjacent longitudinal veins, supporting the vein framework as a whole. Together, these veins create a grid-like structure referred to as the 'vein domain' or 'wing geometry'. A well-engineered wing geometry provides tunable local elasticity and deformation, improving wing stability and enhancing aerodynamic performance. These benefits are reflected in the high lift-to-drag ratio, flight efficiency, and reduced energy expenditure during flight [9]. Fig. 1(a) shows a typical dragonfly wing geometry, where the cellular shapes and sizes vary considerably. Generally, the veins near the body and along the leading edge are thicker and stronger, providing greater rigidity [10]. The corresponding local vein cells often have a square or elongated rectangular geometry (low circularity) vertical to the wing edges, helping to support external
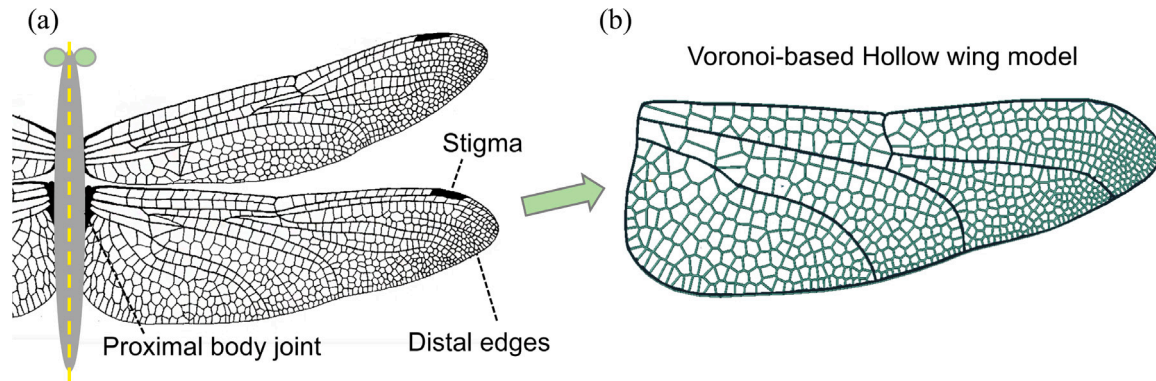

Fig. 1. Illustration of a typical vein structure in a dragonfly wing. (a) Re-imaged wing of an anisopterous dragonfly (Libellulidae), as referenced in [7]. (b) Main vein boundaries (black) and subdomains (green) of the Voronoi-tessellation rear wing sample.

drag loading during the flight. Conversely, veins towards the distal side and trailing edge are thinner and more compliant, with the vein cells in these regions typically exhibiting pentagonal or hexagonal shapes (high circularity). These features ensure sufficient stability even in the rear wing regions, which typically experiences complex twisting deformation and various, multi-directional stresses [11]. In addition to mechanical strength, biological needs also influence vein characteristics in localized regions. For instance, veins typically transition from thick and singular to thin and highly branched as they extend from the body to the distal trailing edges, enhancing nutrient transport efficiency in areas distant from the body. Correspondingly, pore size generally decreases from large near the body to smaller near the trailing edges [12].

From a topological perspective, the dragonfly wing pattern closely resembles patches of Voronoi tessellations. The Voronoi pattern is frequently found in natural materials such as shells, bones, and porous implants, known for their high stiffness and lightweight characteristics [13–15]. Research interests in Voronoi diagrams expanded significantly in the 1990s when Du et al. demonstrated a wide range of applications for centroidal Voronoi tessellations (CVTs), including image compression, quadrature, finite difference methods, resource allocation, cellular biology, statistics, and animal territorial behavior [16]. Over the past two decades, advancements in computer-aided design (CAD) have further refined Voronoi tessellation algorithms, extending their applicability to clustering analysis in diverse fields, including neural networks, pattern recognition, machine learning, computer graphics, and combinatorial chemistry [14]. Fig. 1(b) presents a Voronoi-tessellated model of a dragonfly wing, where Voronoi seeds are positioned to align with the pore centers observed in the natural wing, as shown in Fig. 1(a). While the pore units along the boundary in Fig. 1(a) exhibit slight differences in stretching compared to Fig. 1(b), the central region maintains significant geometric similarity in terms of pore arrangement and area. Additionally, distinct clustering patterns are observed among different vein cells, leading many biological studies to classify particular veins as "main veins" to delineate wing regions, as shown by the black curves in Fig. 1(b). Overall, above findings suggest the probability of employing Voronoi-tessellated multiscale optimization to design advanced flapping wings, which can achieve both advanced engineering performance and close geometric similarity to natural wing structures.

Over the past five years, significant advancements in additive manufacturing have enabled the creation of sophisticated porous lattice structures [17–21], greatly encouraging the development of a new generation of bio-inspired flapping wings [2,22]. Among these advancements, several novel studies have explored dragonfly-inspired design methodologies [2,9,23]. These wing designs aim to replicate key

characteristics of natural dragonfly wings, such as high stiffness, low weight, high natural frequency, and advanced aeroelasticity, through optimization methods. While optimizing traditional static metrics like global stiffness and natural frequency is relatively straightforward in topology optimization, enhancing aerodynamic performance remains a challenge due to its complex mechanisms. For instance, one widely recognized phenomenon in flapping flight, known as "delayed stall", differs significantly from the aerodynamics observed in fixed-wing (rigid-body) flight. In fixed-wing systems, the critical angle of attack (AoA) typically occurs around 16°, with severe stall risks beyond this AoA. In contrast, although dragonfly flapping wings lacking asymmetric airfoils and thus possessing a lower intrinsic lift coefficient, it can often operate effectively at AoAs exceeding 50° without obvious stall effects. Studies suggest that specific flexible deformations in flapping wings are crucial for achieving this phenomenon [24,25]. As flapping wings sweep through the fluid at high AoAs, a leading-edge vortex forms, which result in stable lift [26–29]. This vortex subsequently evolves into smaller separation vortices along the wing, effectively creating a pseudo-smooth surface that helps reduce drag [30]. This entire process allows the wing to sustain movement for distances up to three to five times the wingspan before the separation vortices dissipate. Such phenomena afford insects greater agility and additional time for positional adjustments compared to fixed-wing aircraft.

The above example suggests that strategically designed local flexibility (stiffness) could be crucial for achieving optimal aerodynamics in flapping wings. From an engineering perspective, maintaining geometric similarity between the designed structure and natural insect wings can directly enhance the local stiffness, thereby indirectly yet effectively improving aerodynamic performance. Consequently, many studies have prioritized imitating natural wing patterns within standard optimization frameworks, under the premise that increased geometric similarity to natural wings correlates with enhanced aerodynamic properties. Current optimization studies primarily fall into two categories: physical metric-driven and image processing-driven approaches. For instance, Lin et al. proposed a multi-objective optimization method incorporating circularity constraints for flapping wings [2]. This approach results in substantial improvements in key physical metrics, such as stiffness, frequency, and lift performance. However, their use of centroidal Voronoi tessellation limited the natural similarity at the wing's anterior vein edges. The corresponding isotropic elasticity for the porous structure also to some extent limits the feasible space for the potential optimally-design [31]. Conversely, Zheng et al. [9] utilized neural networks and image processing techniques to design a dragonfly-inspired wing by minimizing an energy balance objective in a coupled "force diagram space" during a neural network training. Although this method achieved high flexibility and vein pattern similarity to natural
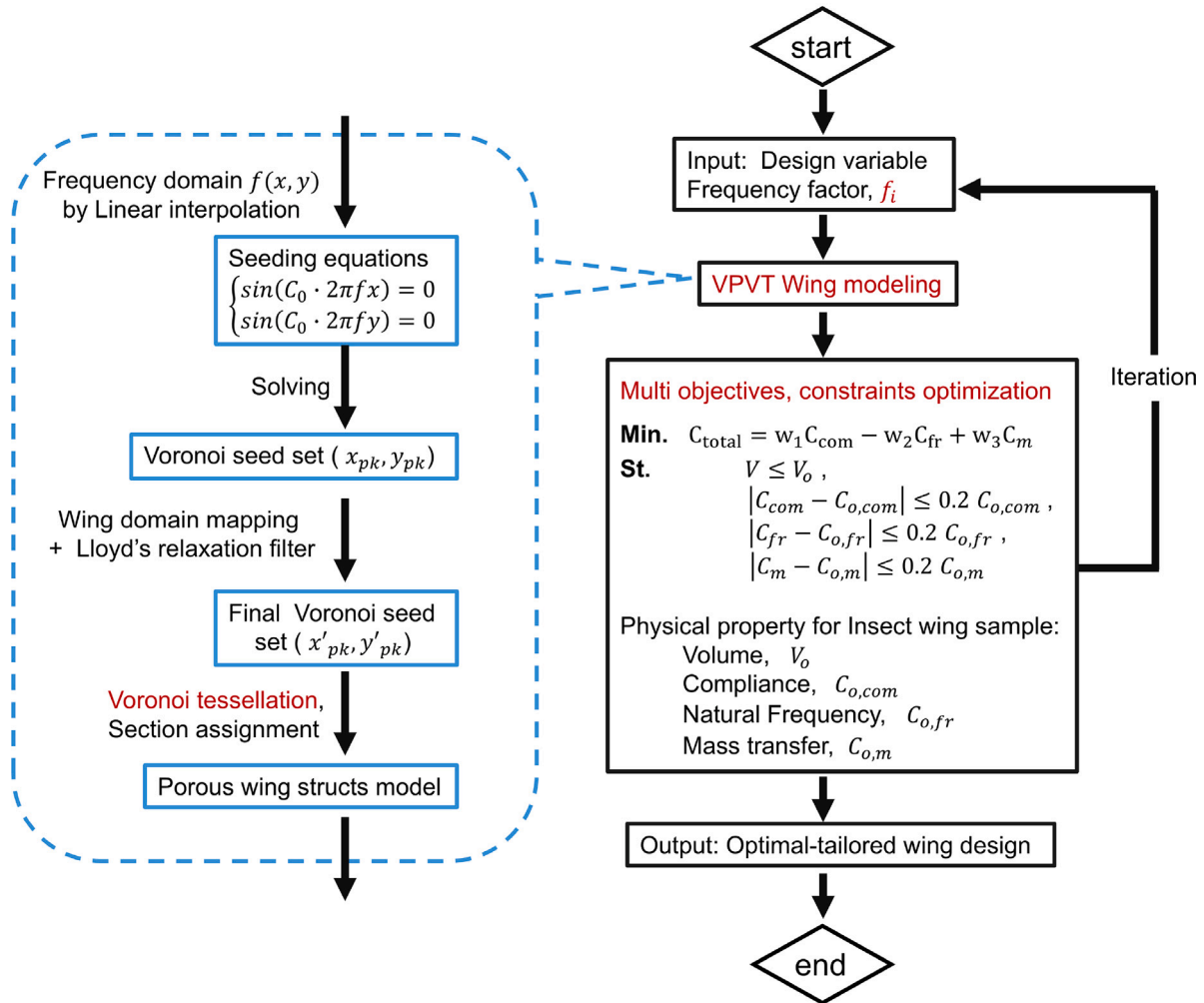
Fig. 2. The workflow VPVT design method for bio-inspired flapping wing.

wings, it did not offer direct control over critical engineering properties such as frequency and total volume, limiting its practical application in industry. These advanced studies underscore the need for an innovative approach that combines practical physical objectives with enhanced natural similarity in the design process.

However, the wing design is technically limited by the two key challenges named 'periodic boundary conditions' and 'scale separation problem' in the structural optimization field. For a porous or lattice structure, existing studies usually use the multi-scale topology optimization to perform the optimally-tailoring for the structure [32–34]. 'Multi-scale' mechanism allows the methods to possess with different micro-architectures and macro-spatial tessellations, thus achieving 'unique micro unit cell' and 'desired global structure performance' [35–37]. However, a number of novel, mainstream multi-scale porous optimization methods are in a multi-lattice mechanism, where using strict constant material presence on the lattice named 'periodic boundary conditions', to promise the connectivity between adjacent topological unit [38–42]. The connectivity interface is with strong artificial characteristics [43,44], and unable to achieve the natural geometry similarity for proposed bio-inspired wing problem.

Compared to these methods, a number of other multi-scale porous optimization have used special porous partition techniques, like Voronoi tessellation, to achieve non-periodic, irregular unit interface [31,45–47]. Although this method certainly address the periodic

boundary constraints, they commonly face with the 'scale separation problem'. To bridging the continuum mechanics in both macro- and micro-scales FE model, the mutliscale optimization usually use homogenized, effective modulus property of macro-scale unit to replace the practical elasticity of the complicated micro-architecture [21,32, 45–49]. In this way, these methods commonly require enough gap separation between micro-scale pore unit and macro-scale design domain, to ensure the accurate homogenization computation [50–52]. However, the proposed wing design problem is a typical multiscale lattice (porous) structure where is more suitable for a meso-macro rather than micro-macro scale configuration. When pore sizes are relatively large compared to the overall design domain, the insufficient separation between pores leads to inaccurate evaluations of the porous structure's effective elasticity. Consequently, conventional multi-scale optimization methods are not applicable to design such porous configurations.

In contrast, Variable-periodic voronoi tessellation (VPVT) method is a novel, bio-inspired design method for porous structures and materials recently proposed by present authors [43]. This method applies an optimally-tailored mechanism to design nature-mimicking porous structures, with strong anisotropic, non-periodic porous geometry and various functional performances. It surpasses the typical isotropic Voronoi but achieves non periodic, bio-similar porous design without artificial-like boundary among topological units' interfaces. Further, due to using
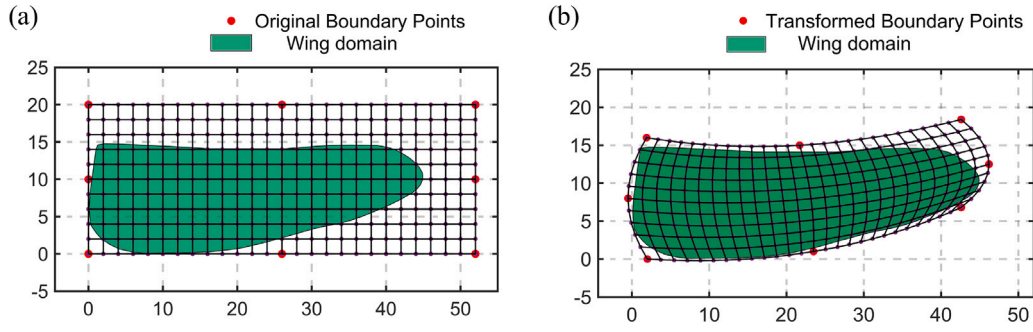
Fig. 3. The configurations of the design domain of the VPVT frequency factors for a flapping wing: (a) the original rectangular design domain; (b) the transformed wing domain. Red points indicate vertices used for domain mapping via shape function interpolation. The green area represents the standard wing geometry, and only Voronoi seeds within this region are taken into account during the VPVT optimization process.

efficient design variable, i.e., frequency factor, for the topological unit, the corresponding topological problem is transferred into parametric optimization problem by global evolution technique. The mechanism thus avoids common homogenization computation in the workflow, ensuring its accuracy for not only micro-macro scale, but also meso-macro scale problem [43]. In this way, it can greatly address the above 'periodic boundary conditions' and 'scale separation' problems discussed above, which suggests strong advantageous in designing flapping wing with advanced physical performance and flight maneuverability.

In this work, we apply the VPVT method combined with a meso-macroscale, multi-objective optimization framework to design bio-inspired flapping wings for micro air vehicles. The VPVT approach optimizes key mechanical objectives, such as stiffness and natural frequency, while incorporating a mass transmission sub-objective to enhance the morphological similarity of the vein pattern. The resulting design demonstrates significant improvements in static mechanical performance, along with potential aerodynamic benefits attributed to its bio-inspired pore structures. This study not only offers insights into the structural determinants of biological wings but also provides detailed models suitable for practical applications in micro air vehicles or delivery robots, which possess superior performance and manufacturability.

In Section 2, the fundamental principles of the VPVT design methodology are firstly introduced, followed by a detailed demonstration of the specialized multi-objective optimization framework and aerodynamic finite element modeling approach employed for the wing design problem. Section 3 presents the final results, including the geometric characteristics and performance evaluation of the optimized wing design, along with a comparative discussion against other advanced studies. Finally, Section 4 summarizes the key findings and conclusions of this study.

2. Methods

This section outlines the methodology of the proposed VPVT approach. Initially, the fundamental principles underlying the VPVT method are presented. Subsequently, an enhanced design process incorporating multi-objective configurations tailored for flapping wing applications is introduced, as depicted in Fig. 2. Finally, the development of a fluid–structure interaction finite element model is presented to validate the design outcomes. Each step is elaborated upon in the following subsections:

2.1. The basic methodology for VPVT design method

The proposed Varying periodic Voronoi tessellation (VPVT) method is an advanced design methodology that leverages global evolutionary optimization to achieve multiscale porous or lattice structure with

desired functionality. In this section, we provide a brief introduction of its fundamental concepts, while for a more comprehensive description please refer to Appendix and our previous work [43].

VPVT is a parameterized optimization approach. For a given design domain, VPVT utilizes a grid partitioning technique to discretize the design space into fundamental quadrilateral representative volume elements (topological units). Each element is characterized by four design parameters located at its vertices, named as frequency factors f_i. Through linear interpolation within each element, the VPVT method can determine the frequency value $f(x, y)$ at any arbitrary point within the entire meshed design domain. Subsequently, applying the seeding equation as Eq. (1), a unique set of Voronoi seeds can be calculated based on the defined design variables f as:

$$|\sin(C_0 \cdot 2\pi f(x, y) \cdot x)| + |\sin(C_0 \cdot 2\pi f(x, y) \cdot y)| = 0 \qquad (1)$$

where the global scale factor $C_0 = 0.1$ is used in this work [43]. All the solutions (x_{pk}, y_{pk}) of the equations will be named as set $\{\mathbf{P}_k\}$, and then used as center points to generate the unique-mapping spatial segmentation pattern through the Voronoi tessellation technique. The method will divides the spatial design domain Ω into several individual Voronoi cells, each of which corresponds to a unique Voronoi seed. For each Voronoi cell R_k, its inner points are closest to its own Voronoi seed compared to any other Voronoi seeds, mathematically defined as [53]:

$$R_k = \{\mathbf{x} \in \Omega | d(\mathbf{x}, \mathbf{P}_k) \leq d(\mathbf{x}, \mathbf{P}_j)\}, \qquad \text{for all } j \neq k$$
$$d(\mathbf{x}, \mathbf{P}_k) = \|\mathbf{x} - \mathbf{P}_k\|_2 = \sqrt{(x - x_{pk})^2 + (y - y_{pk})^2} \qquad (2)$$

where j, k are the indices of Voronoi seeds, $d(\mathbf{x}, \mathbf{P}_k)$ is the Euclidean distance function of Voronoi tessellation. x, y, x_{pk}, y_{pk} are the corresponding spatial coordinates of point $\mathbf{x}$ and Voronoi seed $\mathbf{P}_k$, respectively. Afterwards, by assigning the wireframe of the segmentation boundary with thickness, a typical truss-based porous model can be achieved.

The frequency domain f fundamentally governs the resulting porous structures. By optimizing the design variable f_i associated with the topological units within the domain, the proposed method facilitates the generation of porous architectures with precisely tailored geometries, thereby enhancing performance objectives and enabling diverse functionalities. Fig. A.2 in Appendix further illustrates the VPVT method's capability in modeling geometries with high natural similarity, where the resulting irregular porous structure exhibits strong non-periodic characteristics, closely resembling the intricate patterns observed in dragonfly wing tissues. This sets the VPVT method apart from conventional multiscale design approaches, such as those [38–42] discussed in Section 1. Leveraging this advantage of an expanded design space, VPVT offers a significantly higher potential for achieving a biomimetic and more scientifically optimized flapping wing design compared to other optimization-based tailoring methods.

2.2. Multi-objective VPVT optimization for flapping wings

A standard dragonfly hindwing domain, as introduced in [7], is used to establish the basic design domain for the VPVT flapping wing, as illustrated in Fig. 3. The wing has an average wingspan of 44.1 mm and a chord length of 14.0 mm. To accommodate its complex internal structure, the wing area is divided into multiple discrete sub-design domains along major veins identified in biological classification studies [7,54]. During the VPVT optimization process, each sub-design domain is individually modeled using Voronoi tessellation within the patches defined by its boundaries.

Leveraging the function-driven feature of the proposed VPVT method, the complex, non-structured design domain of the wing sample can be efficiently approximated through an additional mathematical transformation [43] of the function. For simplicity, an initial standard rectangular design domain of 52 mm × 20 mm is selected and discretized into 26 × 10 topological units, as shown in Fig. 3(a). This standard domain is then transformed into a non-structured domain, approximately 48 mm × 16 mm in size, to better align with the wing geometry, thereby improving optimization efficiency and effectiveness, as shown in Fig. 3(b). In this process, the solutions of Eq. (1), (x_{pk}, y_{pk}), are replaced by modified mapping values, (x'_{pk}, y'_{pk}), for subsequent Voronoi tessellation. The corresponding mathematical expression is provided below:

$$\left[x'_{pk}, y'_{pk} \right]^T = \begin{bmatrix} N_1(x_{pk}, y_{pk}) & 0 & \dots & N_8(x_{pk}, y_{pk}) & 0 \\ 0 & N_1(x_{pk}, y_{pk}) & \dots & 0 & N_8(x_{pk}, y_{pk}) \end{bmatrix}$$
$$\cdot \left[x'_1, y'_1, x'_2, y'_2 \dots, x'_8, y'_8 \right]^T$$
(3)

where (x_{pk}, y_{pk}) is the seed solution of Eq. (1) within the original rectangular domain. The modified coordinates, (x'_i, y'_i), correspond to the red vertices of the reshaped domain, as marked in Fig. 3(b). N denotes the corresponding quadratic interpolation shape function of the domain, expressed as follows:

$$\begin{cases} N_1 = \frac{1}{4}(1-\xi)(1-\eta)(-\xi-\eta-1), \\ N_2 = (1-\xi^2)(1-\eta)/2, \\ N_3 = \frac{1}{4}(1+\xi)(1-\eta)(\xi-\eta-1), \\ N_4 = (1-\eta^2)(1+\xi)/2, \\ N_5 = \frac{1}{4}(1+\xi)(1+\eta)(\xi+\eta-1), \\ N_6 = (1-\xi^2)(1+\eta)/2, \\ N_7 = \frac{1}{4}(1-\xi)(1+\eta)(-\xi+\eta-1), \\ N_8 = (1-\eta^2)(1-\xi)/2, \end{cases} \quad \text{where} \begin{cases} \xi = 2(x_{pk}-x_l)/(x_u-x_l)-1, \\ \eta = 2(y_{pk}-y_l)/(y_u-y_l)-1 \end{cases}$$
(4)

where ξ and η are formal coordinate of the solutions (x_{pk}, y_{pk}). x_l, x_u, y_l, y_u correspond the lower or upper bounding of the original rectangle domain in either horizontal or vertical direction.

In this study, only VPVT frequency design variables, and consequently the porous topology, are considered during the optimization process, while the corresponding vein thickness is simplified as a constant. In addition, frequency factors within $y \geq 15$ region is restricted to a single value in order to achieve more rectangular pores in the anterior costal vein region in the corresponding VPVT model [43]. In summary, the total number of design variables is 217, which is an acceptable range for the developed Surrogate-assisted classification-collaboration differential evolution (SaCCDE) optimization method [43]. The population size is set to 40 cases per iteration. The other settings are the same as in [43] by default. In addition, the Voronoi seeds (x'_{pk}, y'_{pk}) are slightly filtered by a Lloyd's relaxation algorithm (1 iteration, 0.2

relaxation factor) before the final Voronoi tessellation processing to further improve the local uniformity and smoothness of the geometry model [55], thereby enhancing its resemblance to the natural wing structure.

Although the vein domain of a dragonfly wing is considered to be an advanced optimal structure, replicating this bio-inspired design using conventional structural optimization methods, such as the SIMP method or other multi-scale topology methods, remains challenging. This difficulty arises from the fact that the natural wing design objectives usually do not only considered the compliance effect, but encompass multiple functionalities and requirements in the process. To achieve both comprehensive performance benefits and a high degree of similarity to natural wing structures, the objectives and constraints for the optimization are defined as Eq. (5) in this work:

$$\begin{aligned} \min \quad & C_{total} = w_1 C_{com} - w_2 C_{fr} + w_3 C_m \\ s.t. \quad & V \leq V_o \quad , \\ & |C_{com} - C_{o,com}| \leq 0.2 C_{o,com} \quad , \\ & |C_{fr} - C_{o,fr}| \leq 0.2 C_{o,fr} \quad , \\ & |C_m - C_{o,m}| \leq 0.2 C_{o,m} \end{aligned}$$
(5)

where the comprehensive objective index C_{total} includes multiple terms, namely bending compliance (C_{com}), base frequency (C_{fr}), and matter (nutrient) transportation capacity (C_m), as referenced in [2]. The weight factors $[w_1, w_2, w_3]$ for the three terms are set to $[500, 1, 0.5]$ in this work, respectively, to ensure balanced normalization. Overall, C_{total} indicates an optimization direction aiming for high stiffness, high natural frequency, and efficient mass transport in the design. Typically, the first two objectives, C_{com} and C_{fr}, represent physical performance metrics with direct engineering significance in wing structure design. The third term, C_m, accounts for a biological factor to enhance the geometric similarity to natural wing structures in this work. To further ensure that the optimized design closely resembles the natural sample, four constraints are applied: the volume of the designed structure v must not exceed the sample volume V_o, and C_{com}, C_{fr}, and C_m are limited within a 20% deviation from the sample performance metrics ($C_{o,com}$, $C_{o,fr}$, $C_{o,m}$), respectively.

Specifically, the sub-objectives C_{com}, C_{fr}, and C_m are calculated as follows:

$$\begin{aligned} C_{com} &= \mathbf{F}^T \mathbf{U}, \quad \mathbf{U} = \mathbf{K}^{-1} \mathbf{F}, \\ C_{fr} &= \min\{\sqrt{\lambda}/(2\pi)\}, \quad \mathbf{Kx} = \lambda \mathbf{Mx}, \\ C_m &= \mathbf{P}^T \boldsymbol{\varphi}, \quad \boldsymbol{\varphi} = \mathbf{K}_t^{-1} \mathbf{P} \end{aligned}$$
(6)

where $\mathbf{F}$ and $\mathbf{U}$ are the nodal force and displacement vectors for the FEM model in the C_{com} equation, and $\mathbf{K}$ is the corresponding elasticity stiffness matrix in continuous mechanics. For the C_{fr} equation, $\mathbf{x}$ and λ are the corresponding eigenvector and eigenvalue of $\mathbf{K}$, respectively. The corresponding topology optimization methodologies for the first two objectives are relatively standard and typical, refer to [56–58]. In contrast, the sub-objective for nutrient transport capacity, C_m, is relatively novel and is calculated following an equivalent 'conductive heat topology optimization approach', where mass transport through the veins is treated analogously to steady heat conduction problem [59]. In this context, the matter-input loading vector $\mathbf{P}$ and nodal matter concentration vector $\boldsymbol{\varphi}$ in Eq. (6) correspond to heat flux loading and nodal temperature, respectively. $\mathbf{P}$ represents the rate of nutrient transport (in moles per second) at inlet nodes, while $\boldsymbol{\varphi}$ indicates the nutrition concentration level at specific node points. The symmetric matter conductivity matrix K_t is analogous to the heat conductivity matrix. As such, a lower C_m indicates more efficient nutrient dissemination within the vein system.

The practical FE computations for Eq. (6) are performed using ABAQUS software (ver.20, Dassault Co., Ltd). The boundary configurations are demonstrated in Fig. 4. For the compliance objective C_{com}, as shown in image (a), the vein branches on the left proximal-body
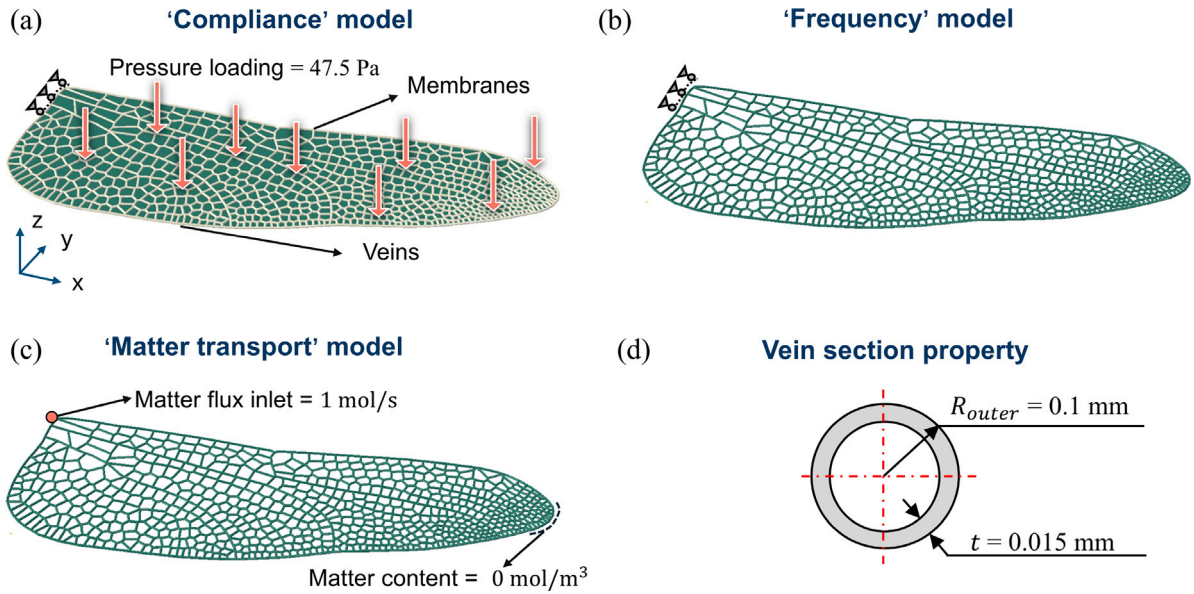
Fig. 4. The configurations of boundary condition for different sub-objective FEM computation. (a) Compliance. (b) Natural frequency (c) Matter transporting. (d) The section definition of the veins beam in FE model.

Table 1
The material property for FEM model configuration [2].

Material	Density	Young's modulus	Poisson ratio	Mass conductivity
Vein	1330 kg/m³	60.5 GPa	0.25	1 mol/s m
Membrane	1190 kg/m³	2.0 GPa	0.25	–

side are fixed in all six degrees of freedom. A membrane shell that encompasses the entire wing domain is modeled and tied to the vein structure. The membrane is subjected to a pressure load of 47.5 Pa that is equivalent to about two times of the dragonfly body weight (about 1.1 g [60,61]), for the purpose of simulating steady flight loading. For the natural frequency objective C_{fr}, only the encastre boundary condition and the vein structure rather than membrane are considered (as shown in Fig. 4(b)). For the matter transport objective C_m, a normalized nutrient inlet load of $P = 1$ mol/s is applied at the left proximal-body vertex, simulating nutrient input from the dragonfly's body. Nutrients are assumed to be fully absorbed by the time they reach the furthest distal wing tips, resulting in a matter content value of $\varphi = 0$ mol/m³ at the wing tip edges. In context of steady mass transfer performance, C_m in Eq. (6) is computed as $C_m = P_i \cdot \varphi_i$.

Although studies indicate that the cross sections of the veins of the dragonfly wing are not perfectly circular but are instead hollow or irregular [62], a simplified constant-diameter hollow section is used in this study for computational efficiency, as illustrated in Fig. 4. The finite element beam elements are generated with an average mesh density of 1.5 mm, and the physical properties [2] along with normalized nutrient conductivity values are provided in Table 1. Notably, the term "Mass Conductivity" is introduced as an analog to "Heat Conductivity", representing the number of moles transported per second per unit distance.

2.3. The FE model for aerodynamics validation

After optimizing the wing structure, the geometric model, covered by a membrane skin, is subjected to FEM simulations to validate its aerodynamic advantages. Compared to conventional MAV designs, a distinctive feature of dragonflies is their better ability to perform complex maneuvers—such as quick stops, gliding, hovering, and diving—while maintaining high energy efficiency. This performance is largely attributed to the wings' ability to sustain a high lift coefficient with varied drag coefficient during such actions when even at large angles of attack. To capture this capability, fluid–structure coupling simulations (Ansys Co. Ltd, ver. 19) are used to replicate the practical gliding behavior of dragonflies. In the simulation setup, the VPVT wing model is tested at various angles of attack within an Eulerian domain under low Reynolds number flow conditions ($Re \leq 1000$), with an inlet velocity of 10 m/s. To simulate a stable gliding process and ensure solution convergence, the total time step is set to 0.1 s—approximately 2–3 times the duration of a typical flapping cycle. For the solid model configuration, the wing structure is fixed at the upper-left side, as shown in Fig. 5(a), to represent the relative stability of the dragonfly's body during gliding. Additionally, minor modifications are made to the wing shell's proximal side to align it with the symmetry boundary condition (SYMM) in the fluid model. The fluid model is created using FLUENT software (Ansys Co. Ltd, ver. 19) with the "$Realizable, K - \epsilon$" viscosity model and a scalable wall function to emulate the low-speed, laminar flow environment typical of dragonfly gliding. The dimensions of the Eulerian domain are set to 200 mm × 300 mm × 150 mm, as illustrated in Fig. 5(b). The mesh around the wing surface is refined to a minimum density of 0.1 mm, as shown in Fig. 5(c). The membrane shell in the transient structural module and the membrane wall in the FLUENT module are coupled to facilitate efficient data transfer between the solid and fluid domains. Further, a typical truss-lattice wing design from the MAC industry, shown in Fig. 5(d), is also included in the simulation for comparison. Both the VPVT-designed wing and the truss-lattice wing have the same volume, while the latter featuring a circular cross-section of 0.105 mm in radius.

3. Results and discussions

This section presents the results of the VPVT optimization process and the final optimized wing structure. Section 3.1 focuses on the geometric topology of the optimized design, providing a comparative analysis with a natural wing sample. Section 3.2 examines the
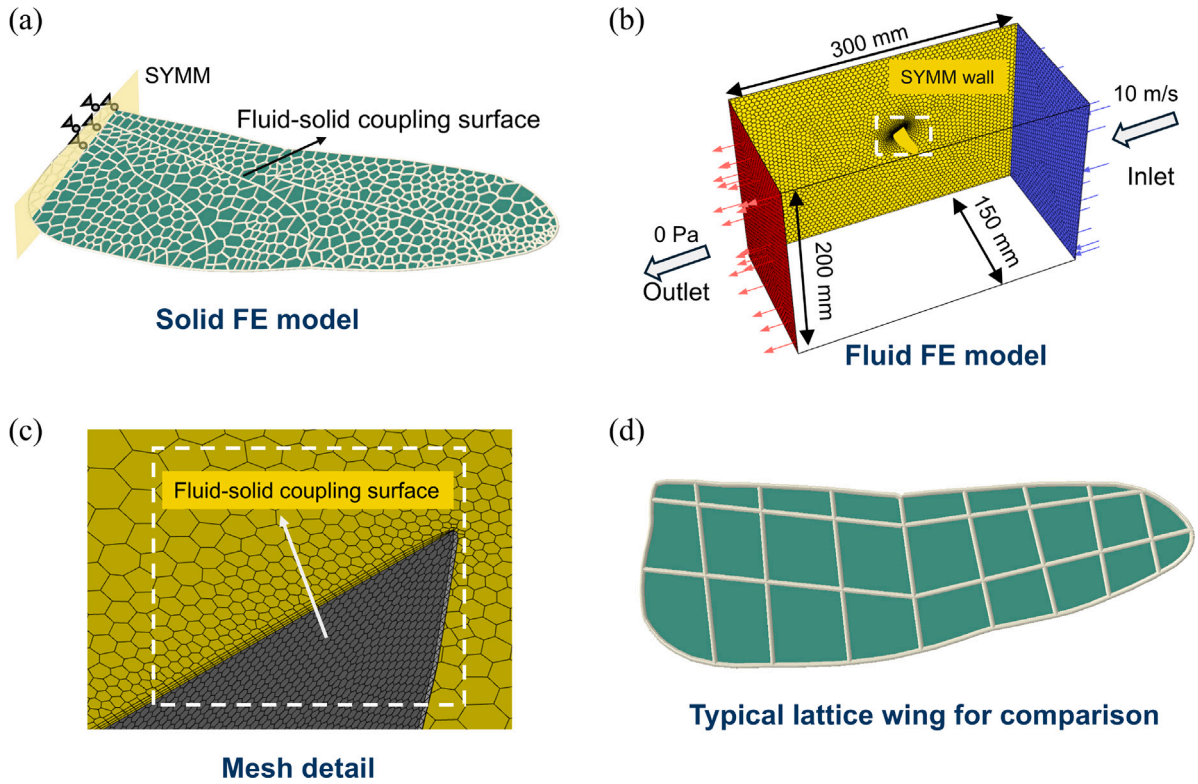
Fig. 5. The configurations of FE models for the aerodynamic validation: (a) transient solid model; (b) fluid model, (c) mesh density around the wing, and (d) a typical truss-lattice wing model for comparison.

fundamental physical properties of the design, while Section 3.3 investigates its aerodynamic characteristics and the underlying mechanisms governing its performance.

3.1. The natural-mimicking geometry

The convergence history, illustrated in Fig. 6, demonstrates the effectiveness of the proposed VPVT method. The total objective value saw a 46% reduction after optimizing 2520 populations (63 generations), with the volume remaining stable at the 10 mm³ constraint. The small generation (iteration) number and good constraint convergence suggest the good effectiveness and efficiency of the proposed method for this expensive problem [63,64]. The convergence of the three sub-objectives, shown in Fig. 6(a), indicates improvements in all specific performance metrics compared to the natural wing, with the variations of −19.6%, 12.5%, and −5.2% in C_{com}, C_{fr} and C_m, respectively. Four critical points in the optimization process are highlighted in Fig. 6(b). The optimized structure all exhibits a high degree of visual resemblance to the natural counterpart, featuring pentagon or hexagon-shaped pores in the posterior region and quasi-rectangular cells near the anterior longitude vein.

Fig. 7 provides further evidence of the geometric similarities by comparing the cell area and circularity between the natural wing and the final optimized design (optimal case 4 in Fig. 6). The two models exhibit comparable average pore areas of 0.52 and 0.57, and circularity values of 0.77 and 0.79, respectively, indicating consistency in structural characteristics. As shown in Fig. 7(a), both designs feature quasi-rectangular cells aligned perpendicular to the boundary in the front costal vein region, while the distal, rear region predominantly consists of hexagonal and pentagonal cells. Correspondingly, the circularity increases progressively from the proximal front wing–body connection to the distal rear wing tip. This arrangement aligns with an engineering rationale: the front edges of the wing require high stiffness to withstand significant fluid drag and maintain stability during

flight. The rectangular vein network reinforces the wing's ability to resist high air pressure along the chord direction, reducing the risk of global buckling or fracture. In contrast, the rear posterior wing region in the dragonfly sample is relatively flexible, exhibiting lower local stiffness. This flexibility allows the wing to bend and deform during flight, generating varying air vortices that facilitate complex maneuvers such as sprinting, hovering, or stopping. The hexagonal isotropic pore structure in this region provides the necessary robustness to adapt to multi-directional forces effectively.

Beyond mechanical factors like stiffness and natural frequency, pore density and size play a crucial role in the mass transport objective. As shown in Fig. 7(b), both models exhibit a overall trend of decreasing pore size and increasing density from the proximal wing root to the distal tip. This pattern, which aligns with fundamental physical principles for enhancing mass transfer, mimics natural branching structures such as tree roots or heat conduction pathways. In these systems, branches near the source (e.g., material inlet or heat source) are thicker and fewer, gradually becoming finer and more numerous towards the periphery [59]. This configuration facilitates efficient mass transport and ensures balanced material distribution. Further, our study found that excluding the mass transport objective in optimization resulted in fewer, larger pores at the wing extremities.

However, it is also noticeable that the pore size at the proximal body–wing connection region of VPVT-optimized model is much smaller than that of natural wings. The reason main lies in the simplification of optimization for vein thickness factor in this work. The wing root region is usually considered as high local stiffness to ensure flight stability. While natural wings can achieve this with a sparse yet thicker vein network, the optimized design, constrained by uniform thickness in proposed optimization configuration, can only compensates the local stiffness through increasing pore density in the region. Under this, two samples finally show to some extent different in the geometry. Besides, the work ignores some complicate mechanical features of vein like section corrugation [65,66], which also induce the divergence in
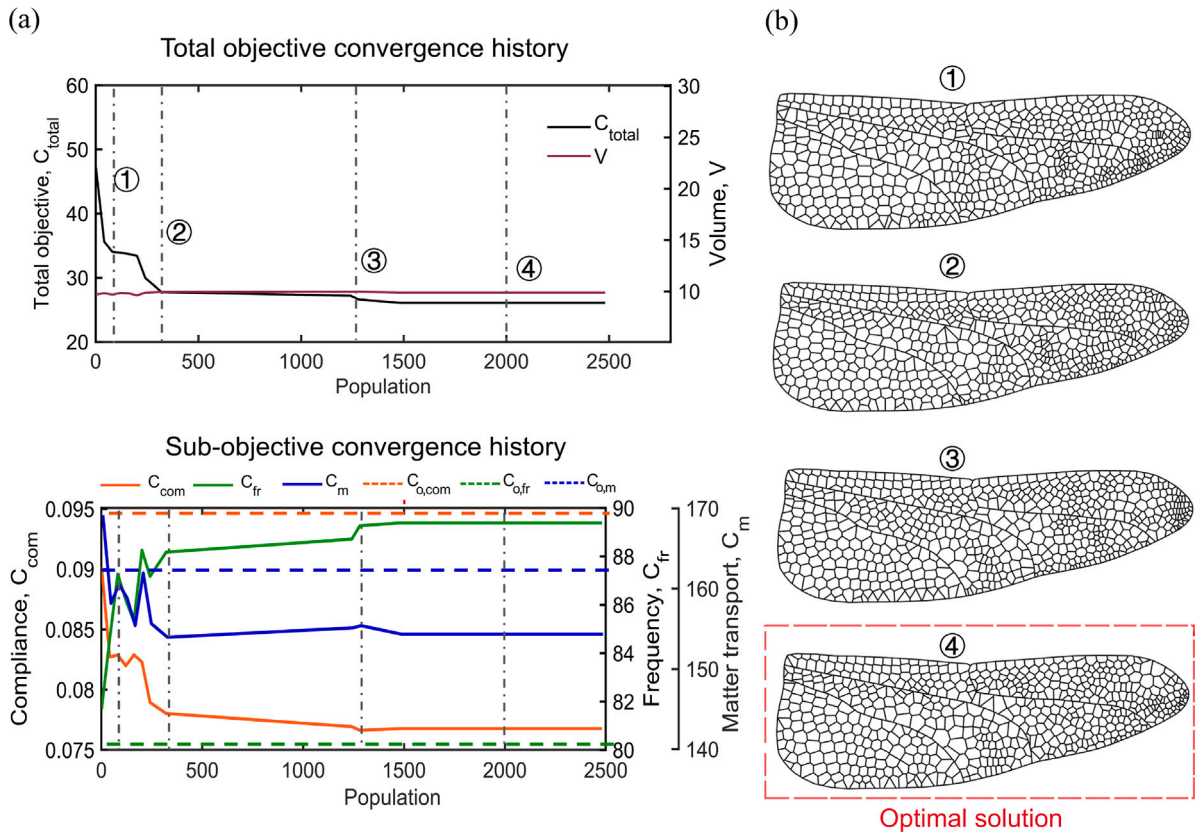
Fig. 6. The configurations of boundary conditions for different sub-objective FEM computations: (a) Compliance, (b) Natural frequency, (c) Mass transport, and (d) Cross-sectional definition of the vein beams in the FE model.
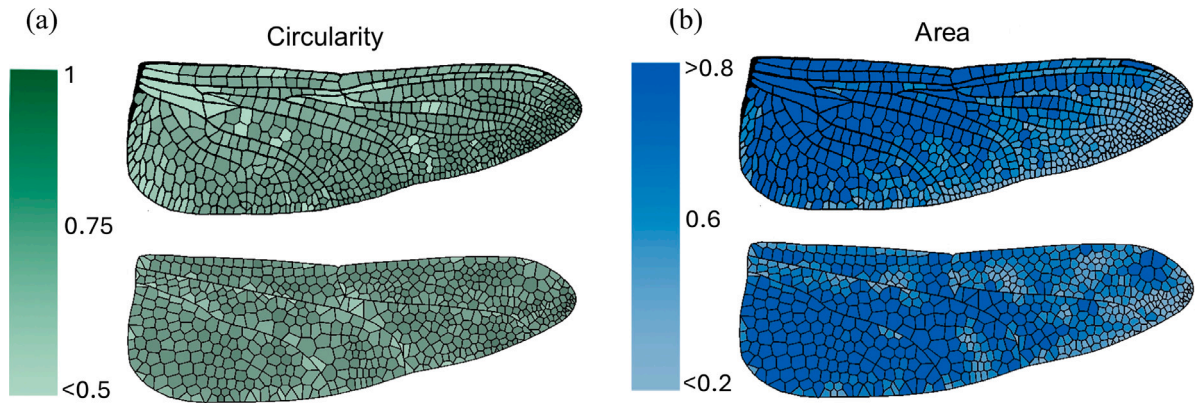

Fig. 7. The geometry comparison of between natural sample (upper) and designed wing (bottom). (a) the cell circularity. (b) the cell area.

the proximal geometry of both the VPVT wing and the natural wing. Despite this, as the VPVT wing eventually presents a better compliance performance than the natural sample, we still consider the optimized solution is advanced and acceptable in this work. In addition, future studies may incorporate vein thickness and stigma weight as additional variables in optimization to further enhance the geometry similarity.

3.2. The optimized physical performance

Fig. 8 presents the detailed FEM simulations of the optimally-designed flapping wing using the VPVT method. As outlined in Section 2, the optimized frequency domain is shown in Fig. 8(a), in which the unique value constraints applied in the upper domain. The deformation behavior of the dragonfly wing under pressure, shown in Fig. 8(b), demonstrates a realistic beam-bending mode. In this way, the

maximum deflection occurs at the wing tip, a characteristic consistent with observations by [67,68]. This evidences the enough flexibility (stiffness decrease) of the structure along the wingspan direction.

The first three frequency modes, depicted in Fig. 8(c), (d), and (e), reveal key dynamic characteristics of the optimized wing. The first mode involves spanwise bending, a fundamental mode for flapping wings. Subsequently, the maximum displacements occur at the middle of the trailing edge and tip edges near the leading side in mode 2, and at the middle of the leading edge and tip edges near the trailing side in mode 3. This deformation behavior aligns well with the vibration study results of real dragonfly vein networks by Rajabi et al. [69]. This consistency implies the scientific foundation of our bio-inspired VPVT design, highlighting its potential to advanced flight performance. Furthermore, the significant frequency gap between the first and second
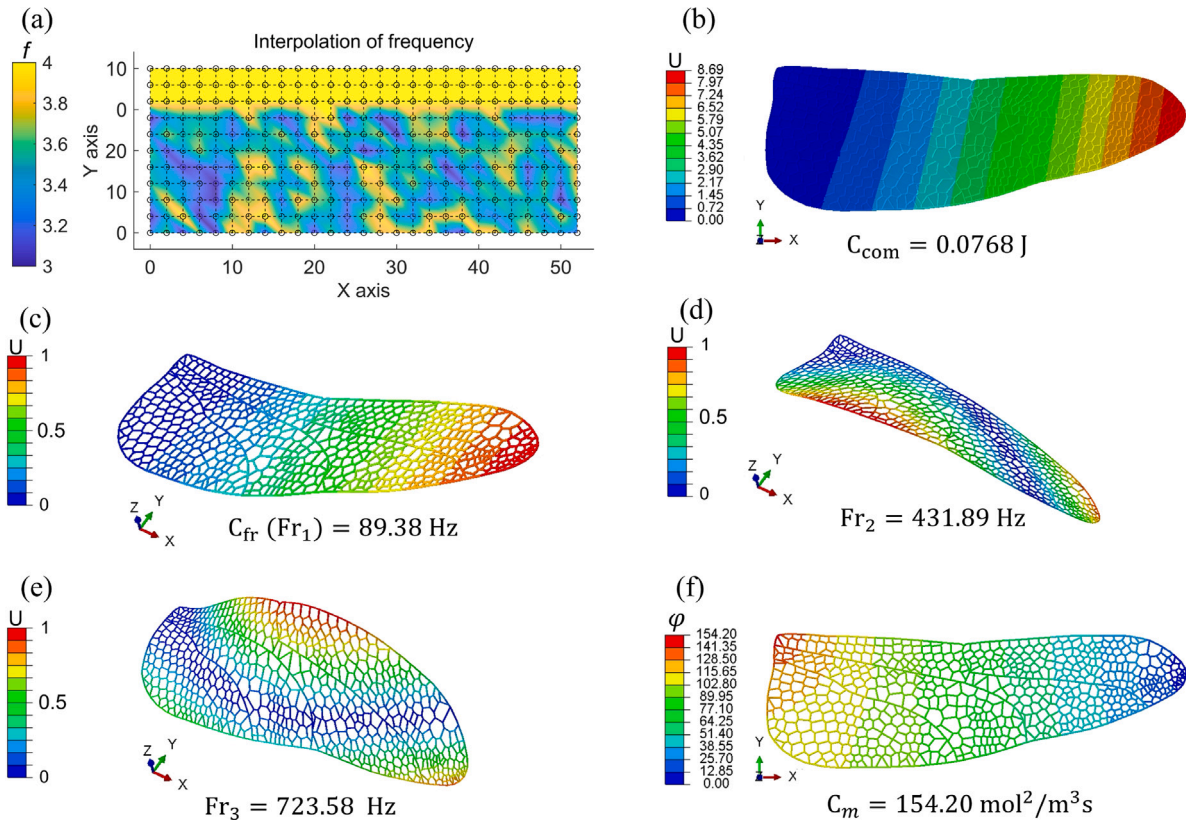
Fig. 8. The results of FEM computation for the optimized VPVT wing. (a) The final optimal solutions f of VPVT optimization. (b) The compliance performance. (c),(d),(e) The first three order natural frequencies of the wing structure. (f) The steady matter concentration in vein system after mass transportation.

modes indicates a lower risk of mode-switching or mode-jumping [70], thereby implicitly suggesting both numerical optimization robustness and flight stability under airflow.

The mass transfer results are presented in Fig. 8(f), in which the concentration distribution of nutrition matter decreases uniformly along the wing span. It suggests that the nutrition concentration is initially maximum at body inlet, then gradually transferred and absorbed by vein system, finally completely consumed on the distal tip side. This solution is in accordance with the typical biological principles and, as a result, we consider this design to be scientific valid. Further, given that the rear vein edges of natural wings are often thin or even absent, which reduces mass transfer efficiency, future studies should consider implementing additional localized constraints of $\varphi = 0$ mol/mm^3 in these regions instead of only at the wing tip vertex. This adjustment will further reduce pore size along the trailing wing edges.

3.3. The optimally-tailored aerodynamic performance

This section presents the aerodynamic analysis of the VPVT wing, comparing its performance with conventional lattice wings and real dragonfly wings. The aerodynamic simulation results are illustrated in Fig. 9. Specifically, Fig. 9(a) depicts the variations in lift and drag coefficients (C_l and C_d) for the VPVT wing, the lattice wing, and a real dragonfly wing across different angles of attack (AoA). Both the VPVT and lattice wings exhibit an increasing trend in lift and drag coefficients as the AoA increases from 0° to 40° in increments of 5°. Quantitatively, the VPVT wing achieves an average lift coefficient of 0.65, compared to 0.60 for the lattice wing, while the corresponding average drag coefficients are 0.31 and 0.29, respectively. Furthermore, the attained results demonstrate reasonable agreement with experimental data obtained from natural dragonfly gliding, as reported by Wakeling et al. [61]. In terms of C_l, both studies indicate comparable values and a similar

increasing trend in the low AoA region (0° to 10°), with the growth rate gradually decreasing beyond 10°. Regarding C_d, both studies exhibit a steady increase with a nearly constant slope. This consistency validates the accuracy and reliability of the proposed solid–fluid FE simulation approach.

Despite the notable aerodynamic improvements achieved by the VPVT design, discrepancies remain when compared to real dragonfly wings. Specifically, the proposed results still exhibit an average gap of 15% in lift coefficient at high angles of attack (20°–40°), as shown in Fig. 9(a). From an engineering perspective, this deviation is reasonable and acceptable, given that real dragonfly wings possess far greater structural complexity and functional adaptability than the simplified truss-based framework used in this study. The superior aerodynamic performance of dragonfly wings arises not only from the vein network geometry considered in this work but also from various intricate biomechanical mechanisms, including zig-zag section corrugation [65, 66], one-way hinge nodus connections [71], and forewing–hindwing coupling effects [72,73]. These additional structural features modulate local wing motion and inflow characteristics, ultimately enhancing lift generation and the maneuverability of live dragonflies. In future studies, the VPVT framework will be refined by incorporating more realistic and distinct truss connections within the vein network to better capture deformation behaviors. The corresponding results are expected to show further improvements.

For a more rigorous comparison between the two engineered wings, the normalized differences in aerodynamic performance between the VPVT and lattice designs are presented in Fig. 9(b). The VPVT wing exhibits a 7.29% reduction in drag coefficient C_d at a 5° AoA compared to the lattice wing, while achieving a 9.86% increase in lift coefficient C_l at a 30° AoA. These results highlight the superior aerodynamic performance of the VPVT wing. Notably, the most typical AoA for steady dragonfly gliding ranges from 0° to 15° [61], where a lower
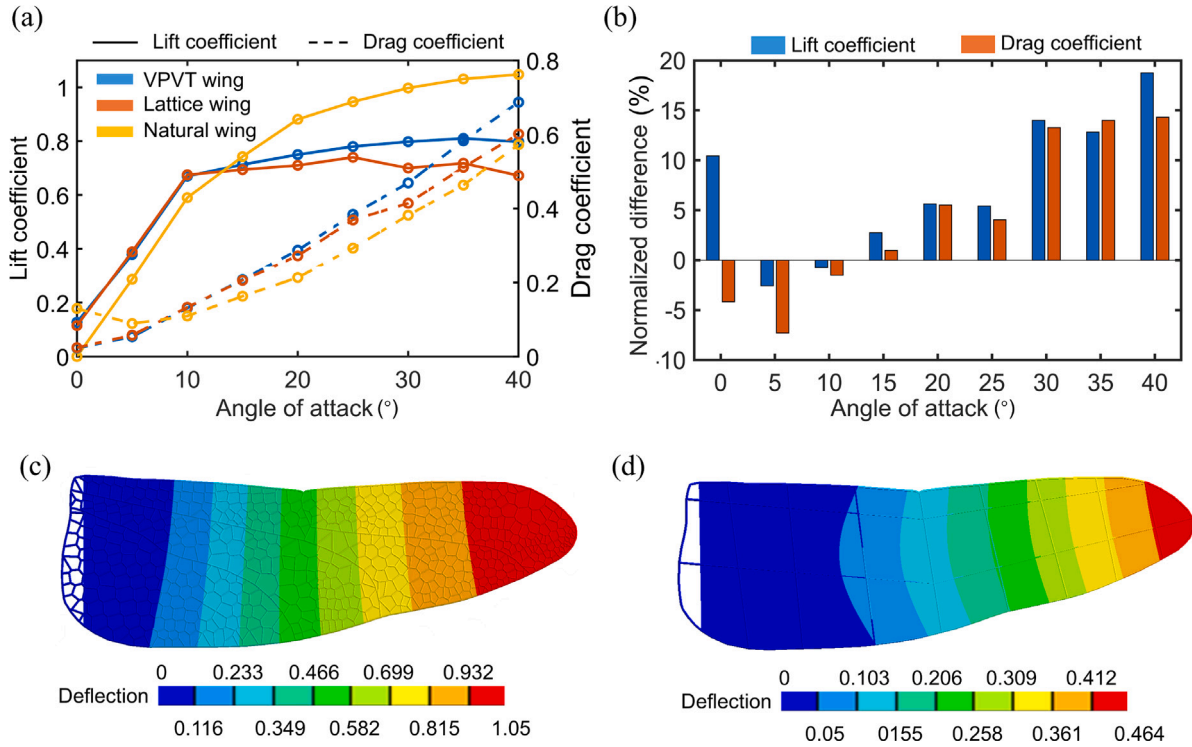
Fig. 9. The Aerodynamic solutions for the VPVT wing, lattice wing. (a) The drag and lift coefficients under different angles of attack, compared to ones of vivo dragonfly measured by [61]. (b) Normalized difference in aerodynamics C_l and C_d, computed in format as $(C_{i,VPVT} - C_{i,lattice})/C_{i,lattice}$. (c) the VPVT wing and (d) the lattice wing deformation (mm) under the air flow pressure of 30° AoA.

drag coefficient is critical for maintaining higher speeds and improving energy efficiency. In this context, the reduced C_d of the VPVT wing at low AoA enhances forward velocity and minimizes momentum loss, making it particularly suitable for micro air vehicles (MAVs) that require extended flight durations and lower energy consumption. Conversely, dragonflies typically fold and adjust their wing roots to a high AoA when performing maneuvers such as emergency stops or sharp turns from a gliding state. In such cases, the higher C_l of the VPVT wing helps prevent stall and facilitates hovering, while its increased C_d aids in rapid deceleration from forward motion. These characteristics suggest that the VPVT wing offers superior maneuverability compared to the lattice wing.

Above gap for aerodynamic between the VPVT-wing and lattice-wing can be explained by the difference in local stiffness for two design. It is reported that the flexible wings can commonly yield higher lift coefficients than rigid wings during flapping flight, especially at high AoA range (20°–40°) [74–77]. Experimental investigations by Kang et al. [76] and Lucas et al. [78] have attributed this enhancement to the passive, non-uniform wing deformation caused by inflow pressure. To illustrate these effects, Fig. 9(c) and (d) compare the deformation patterns of the VPVT and lattice wings at a 30° AoA under aerodynamic loading. The VPVT wing, with its optimized biomimetic local stiffness ($C_{com} = 0.077$), undergoes a more pronounced and advantageous deformation (with maximum deflection 1.05 mm). Its deformation iso-surface contour exhibits a striped pattern along the chord direction with a deflected angle. In contrast, the lattice wing, which has higher structural stiffness ($C_{com} = 0.070$), shows minimal overall deflection along both the span and chord directions (with maximum deflection 1.05 mm). Instead of a continuous deflection, its deformation iso-surface reveals a ripple-like banding pattern (Fig. 9(d)). In this way, the angle of net force vector and center of pressure is considered

systematically vary with respect to above wing flexibility, and finally enhances higher lift force on more flexible wing case [79].

The aforementioned conclusions are further substantiated by Fig. 10, which illustrates the airflow contours around the wings at angles of attack (AoA) of 5° and 30°. At an AoA of 5° (Fig. 10(a)), the wing deformation results in an asymmetric airfoil profile, creating a velocity differential above and below the wing surface. A comparable velocity contour has been reported by Chitsaz et al. [80]. This separation in airflow velocity generates a pressure differential in the leading region of the wing, thereby contributing to lift generation [30]. As the AoA increases to 30° (Fig. 10(b)), laminar flow separation expands and fails to reattach past the trailing edge, leading to turbulence on the upper wing surface. Such turbulence alters the pressure distribution near the trailing edge, enhancing lift through a clockwise twisting effect at the wing's trailing edge [25]. The VPVT design achieves superior local stiffness by maintaining high geometric similarity during the optimization process, resulting in weaker separation of low-velocity regions ($V < 2\,\mathrm{m/s}$) on the upper wing surface compared to the lattice wing. This is inferred to enhance turbulence circulation on the upper wing surface, ultimately improving the lift coefficient [25]. This inference is partially evidenced by the iso-vorticity contour shown in Fig. 10(c). The red leading-edge vortex in the VPVT wing case exhibits a stronger oval shape extending downstream to the trailing edge, in contrast to the striped pattern observed in the lattice wing case. This results in relatively stronger vortices adjacent to the upper wing surface, thereby achieving improved lift performance [30,65].

In summary, the high lift coefficient at high AoA and low drag coefficient at low AoA during gliding highlight the aerodynamic advantages of the VPVT wing design. These characteristics suggest reduced energy loss and increased maneuverability, making the design particularly suitable for micro air vehicles (MAVs) requiring long-duration flights and effective obstacle avoidance. Such features position the VPVT
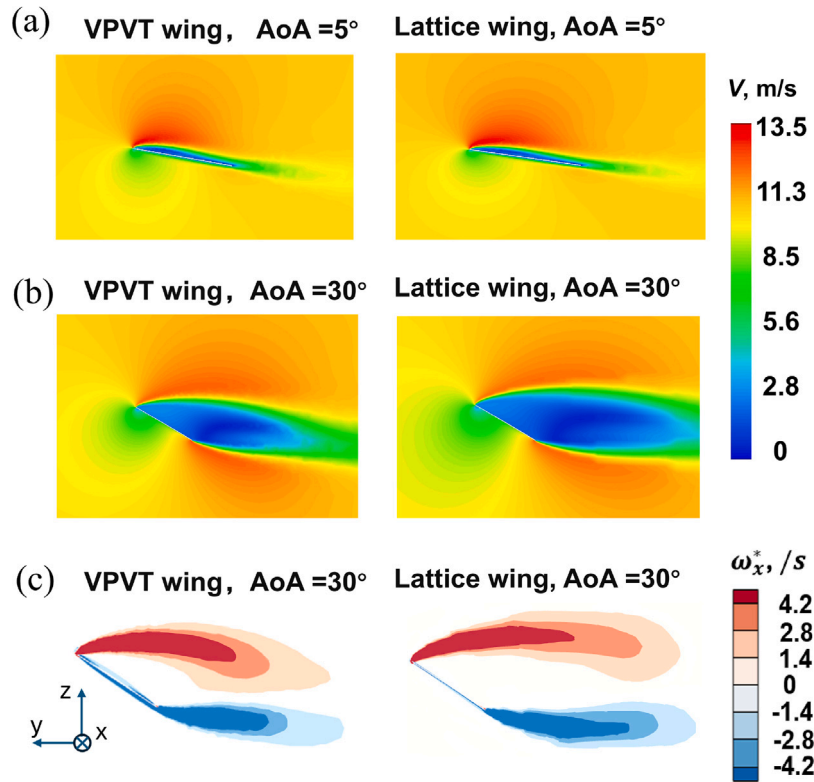
Fig. 10. The airflow contours for the wing section at a distance of 30% of the wingspan from the wing root at transit 0.1 s time point. (a) The velocity magnitude plot at 5° AoA. (b) The velocity magnitude plot at 30° AoA. (c) The normalized vorticity distributions in *x*-direction at 30° AoA. Notably, in (b), the laminar flow does not rapidly reattach after the trailing edge; however, in the context of flapping wings, this is not considered stall, differing from typical fixed-wing studies.
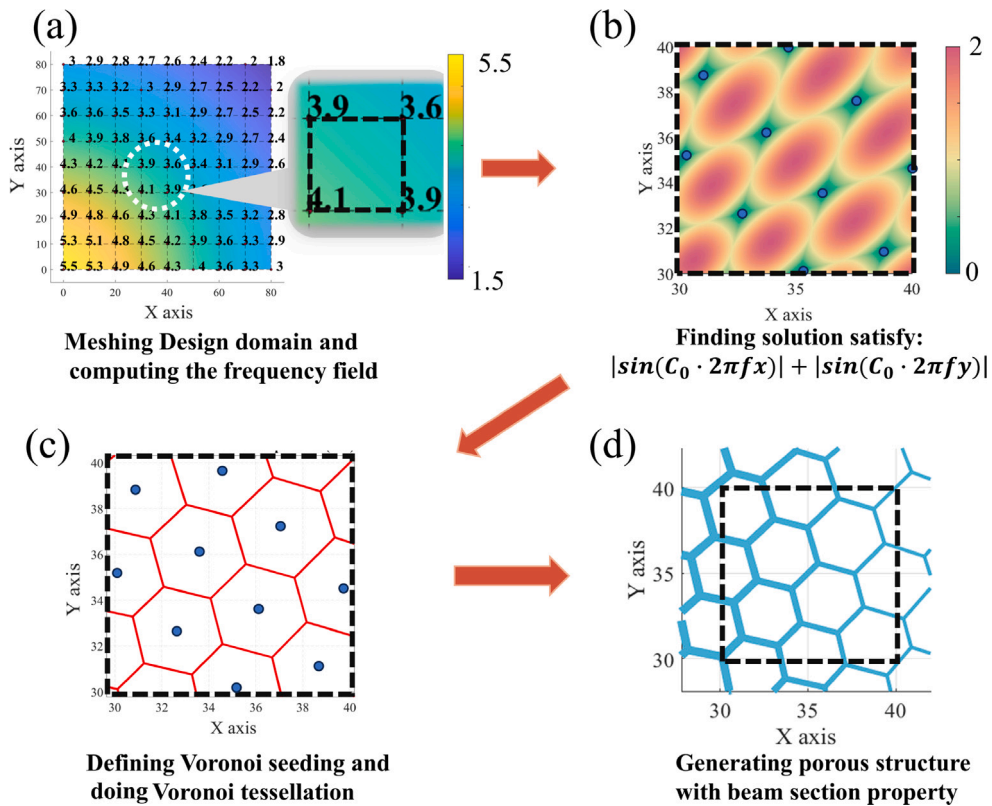

Fig. A.1. The VPVT modeling process, adapted from [43]. (a) The frequency field ƒ among design domain. (b) Solution of the seeding equation for a single topological unit. (c) Generation of the Voronoi seed set and execution of Voronoi tessellation. (d) Formation of the final porous (lattice) structure with defined beam section properties.
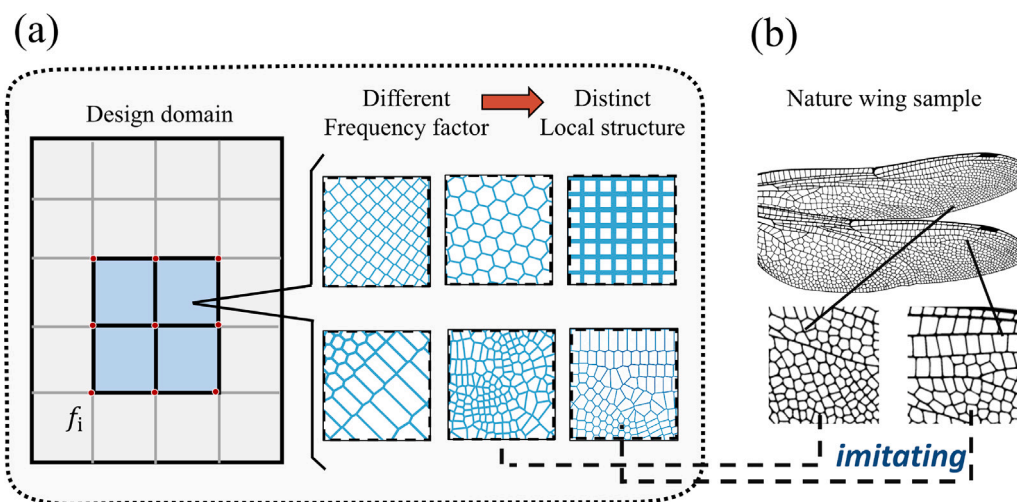
Fig. A.2. The diverse design space enabled by the VPVT method, adapted from [43]. (a) Various porous structures generated by modifying the frequency factor configuration f_i, including diamond, honeycomb, square, irregular foam, and others. (b) Non-periodic topological unit exhibiting high similarity to natural biological patterns.

wing as a promising option for applications like delivery monitoring and search-and-rescue missions. In additions, this study, which differs from asymmetrical fixed-wing designs, highlights that a stiffer structure is not always necessarily optimal for flapping wings. Instead, a bio-inspired flexible wing design that balances local stiffness can further enhance aerodynamic performance. These findings underscore the advantages of the multi-objective VPVT optimization process, which considers not only stiffness and natural frequency but also geometric similarity, leading to a more holistic and effective wing design. Further, compared to other popular bio-inspired wing design method by neural network or image processing methodology [9], the proposed method adopts a mechanic methodology to achieve the final design. On one hand, it significantly decreases both dependence of insect training database and computational costing during the design process. On the other hand, this approach allows for stricter and more explicit constraints on the final physical properties, such as the compliance and volume of the wing, making it more applicable to practical scenarios. By incorporating the proposed multi-objective optimization process, the workflow also offers researchers a deep understanding of the diverse factors that influence insect wing geometry, providing a comprehensive framework for future studies in this field.

4. Conclusions

In this work, a flapping wing with advanced aeroelastic performance inspired by the natural dragonfly wing is developed through the proposed Variable-Periodic Voronoi Tessellation (VPVT) method. The optimization process integrates 'design domain mapping' with a 'multi-objective framework', to obtain the final design of wing structure. The VPVT method successfully generates a wing structure with high geometric similarity to the natural dragonfly wing while delivering significant improvements in key engineering metrics. Specifically, the optimized wing structure demonstrates improvements of 19.6%, 12.5%, and 5.2% in stiffness, natural frequency, and mass transport efficiency, respectively, compared to the natural wing sample.

Aerodynamic performance validation through FEM simulations shows a 9.86% increase in lift force during high-attack angle gliding compared to a conventional lattice-filled wing design. These results highlight advantageous energy efficiency and maneuverability achieved from the proposed method, making it particularly well-suited for long-duration flights and complex maneuvers in MAV applications.

Compared to other popular neural-network-based bio-inspired design methods, the proposed mechanics-based optimization workflow reduces the reliance on insect training datasets and computational

costs, thus enhancing its practical applicability. Additionally, it enables stricter constraints on physical properties like compliance and volume of the designed models, offering deep insights into the factors influencing insect wing geometry. Future research should consider additional design variables, such as vein thickness and refined mass transfer constraints, to further enhance the wing's performance and expand its potential applications.

CRediT authorship contribution statement

Declaration of competing interest

The authors declare that they have no known competing financial interests or personal relationships that could have appeared to influence the work reported in this paper.

Acknowledgments

Appendix. VPVT modeling demonstration and bio-inspired design space

Fig. A.1 illustrates the detailed modeling process using the Voronoi-based Porous Variable Topology (VPVT) design method. Initially, a given rectangular design domain is discretized into several topological units, with corner vertices assigned specific frequency values f_i (Fig. A.1(a)). These values facilitate the computation of a frequency field across the domain via linear interpolation.

For each topological unit, the inner Voronoi seeds are determined using the seeding equation (1), as demonstrated in Fig. A.1(b). Subsequently, the porous geometry is generated by performing Voronoi tessellation based on these seeds throughout the entire design domain,

as depicted in Fig. A.1(c). Finally, the resulting porous structure is completed by defining the truss model with appropriate beam section properties.

Fig. A.2 presents a selection of representative porous structures generated by manually adjusting the frequency factor configuration within the VPVT method. This highlights the extensive design flexibility offered by the proposed approach. Despite employing a limited number of design variables, the method enables the generation of a diverse range of feasible porous geometries. This capability substantially enhances the effectiveness of evolutionary optimization within the VPVT framework, setting it apart from conventional homogenization-based multiscale design methods [43]. Moreover, the latter two irregular lattice structures in Fig. A.2(a) exhibit a remarkable resemblance to natural dragonfly wing patches, further underscoring the VPVT method's potential for bio-inspired and optimally tailored structural designs.

Data availability

Data and codes will be made available at www.m2olab.uk.

References

[1] Jiakun H, Zhe H, Fangbao T, Gang C. Review on bio-inspired flight systems and bionic aerodynamics. Chin J Aeronaut 2021;34(7):170–86.

[2] Lin S, Chou N, Li G, Bao D, Cai Y, Xie YM, Wang G. A gradient-evolutionary coupled topology optimization for sheet reinforcement based on the mechanics of Voronoi pattern on dragonfly wings. Adv Eng Softw 2024;190:103600.

[3] Xiao S, Hu K, Huang B, Deng H, Ding X. A review of research on the mechanical design of hoverable flapping wing micro-air vehicles. J Bionic Eng 2021;18:1235–54.

[4] Hu Y, Ru W, Liu Q, Wang Z. Design and aerodynamic analysis of dragonfly-like flapping wing micro air vehicle. J Bionic Eng 2022;19(2):343–54.

[5] Phan HV, Park HC. Insect-inspired, tailless, hover-capable flapping-wing robots: Recent progress, challenges, and future directions. Prog Aerosp Sci 2019;111:100573.

[6] Chen L, Cheng C, Zhou C, Zhang Y, Wu J. Flapping rotary wing: A novel low-Reynolds number layout merging bionic features into micro rotors. Prog Aerosp Sci 2024;146:100984.

[7] Tillyard RJ, Fraser FC. A reclassification of the order odonata based on some new interpretations of the venation of the dragonfly wing. Royal Zoological Society of New South Wales; 1938, p. 165–73.

[8] Rajabi H, Shafiei A, Darvizeh A, Dirks J-H, Appel E, Gorb SN. Effect of microstructure on the mechanical and damping behaviour of dragonfly wing veins. R Soc Open Sci 2016;3(2):160006.

[9] Zheng H, Mofatteh H, Hablicsek M, Akbarzadeh A, Akbarzadeh M. Dragonfly-inspired wing design enabled by machine learning and maxwell's reciprocal diagrams. Adv Sci 2023;10(18):2207635.

[10] Salcedo MK, Hoffmann J, Donoughe S, Mahadevan L. Computational analysis of size, shape and structure of insect wings. Biology Open 2019;8(10):bio040774.

[11] Combes SA. Materials, structure, and dynamics of insect wings as bioinspiration for MAVs. Encycl Aerosp Eng 2010;7(Part 34).

[12] Salcedo MK, Socha JJ. Circulation in insect wings. Integr Comp Biol 2020;60(5):1208–20.

[13] Deering J, Dowling KI, DiCecco L-A, McLean GD, Yu B, Grandfield K. Selective Voronoi tessellation as a method to design anisotropic and biomimetic implants. J Mech Behav Biomed Mater 2021;116:104361.

[14] Arvizu Alonso AK, Armendáriz Mireles EN, Calles Arriaga CA, Rocha Rangel E. Control of the properties of the Voronoi tessellation technique and biomimetic patterns: A review. Designs 2024;8(5):93.

[15] Tung C-C, Lai Y-Y, Chen Y-Z, Lin C-C, Chen P-Y. Optimization of mechanical properties of bio-inspired voronoi structures by genetic algorithm. J Mater Res Technol 2023.

[16] Du Q, Faber V, Gunzburger M. Centroidal Voronoi tessellations: Applications and algorithms. SIAM Rev 1999;41(4):637–76.

[17] Wu Y, Fang J, Wu C, Li C, Sun G, Li Q. Additively manufactured materials and structures: A state-of-the-art review on their mechanical characteristics and energy absorption. Int J Mech Sci 2023;246:108102.

[18] Ramakrishna D, Bala Murali G. Bio-inspired 3D-printed lattice structures for energy absorption applications: A review. Proc Inst Mech Eng Part L: J Mater: Des Appl 2023;237(3):503–42.

[19] Wang E, Yao R, Li Q, Hu X, Sun G. Lightweight metallic cellular materials: a systematic review on mechanical characteristics and engineering applications. Int J Mech Sci 2024;270:108795.

[20] Deng W, Kumar S, Vallone A, Kochmann DM, Greer JR. AI-enabled materials design of non-periodic 3D architectures with predictable direction-dependent elastic properties. Adv Mater 2024;2308149.

[21] Wu Z, Xia L, Wang S, Shi T. Topology optimization of hierarchical lattice structures with substructuring. Comput Methods Appl Mech Engrg 2019;345:602–17.

[22] Bishay PL, Brody M, Podell D, Corte Garcia F, Munoz E, Minassian E, Bradley K. 3D-printed bio-inspired mechanisms for bird-like morphing drones. Appl Sci 2023;13(21):11814.

[23] Hou D, Zhong Z. Comparative analysis of deformation behaviors of dragonfly wing under aerodynamic and inertial forces. Comput Biol Med 2022;145:105421.

[24] Thomas AL, Taylor GK, Srygley RB, Nudds RL, Bomphrey RJ. Dragonfly flight: free-flight and tethered flow visualizations reveal a diverse array of unsteady lift-generating mechanisms, controlled primarily via angle of attack. J Exp Biol 2004;207(24):4299–323.

[25] Zhang S, Ochiai M, Sunami Y, Hashimoto H. Influence of microstructures on aerodynamic characteristics for dragonfly wing in gliding flight. J Bionic Eng 2019;16:423–31.

[26] Eldredge JD, Jones AR. Leading-edge vortices: mechanics and modeling. Annu Rev Fluid Mech 2019;51(1):75–104.

[27] Chen L, Zhou C, Werner NH, Cheng B, Wu J. Dual-stage radial–tangential vortex tilting reverses radial vorticity and contributes to leading-edge vortex stability on revolving wings. J Fluid Mech 2023;963:A29.

[28] Wu J, Wang K, Chen L. Leading-edge vortex enhancement of a flexible flapping wing with the clap-and-fling mechanism. Phys Fluids 2025;37(1).

[29] Li G, Wu J, Zhang Y, Chen L. Three-dimensional effects of a tandem flapping–fixed wing configuration at low Reynolds number. Phys Fluids 2024;36(11).

[30] Narita Y, Chiba K. Aerodynamics on a faithful hindwing model of a migratory dragonfly based on 3D scan data. J Fluids Struct 2024;125:104080.

[31] Li Z, Wu Z. A novel multiscale design method for porous structures with tunable anisotropy: Varied-shape Voronoi tessellation. Comput Methods Appl Mech Engrg 2024;432:117378.

[32] Wu J, Sigmund O, Groen JP. Topology optimization of multi-scale structures: a review. Struct Multidiscip Optim 2021;63:1455–80.

[33] Ali MA, Shimoda M. Toward multiphysics multiscale concurrent topology optimization for lightweight structures with high heat conductivity and high stiffness using MATLAB. Struct Multidiscip Optim 2022;65(7):207.

[34] Gao J, Cao X, Xiao M, Yang Z, Zhou X, Li Y, Gao L, Yan W, Rabczuk T, Mai Y-W. Rational designs of mechanical metamaterials: Formulations, architectures, tessellations and prospects. Mater Sci Eng: R: Rep 2023;156:100755.

[35] Nguyen M-N, Hoang V-N, Lee D. Multiscale topology optimization with stress, buckling and dynamic constraints using adaptive geometric components. Thin-Walled Struct 2023;183:110405.

[36] Bishara D, Xie Y, Liu WK, Li S. A state-of-the-art review on machine learning-based multiscale modeling, simulation, homogenization and design of materials. Arch Comput Methods Eng 2023;30(1):191–222.

[37] Gao J, Xue H, Gao L, Luo Z. Topology optimization for auxetic metamaterials based on isogeometric analysis. Comput Methods Appl Mech Engrg 2019;352:211–36.

[38] Gao J, Luo Z, Li H, Gao L. Topology optimization for multiscale design of porous composites with multi-domain microstructures. Comput Methods Appl Mech Engrg 2019;344:451–76.

[39] Imediegwu C, Murphy R, Hewson R, Santer M. Multiscale structural optimization towards three-dimensional printable structures. Struct Multidiscip Optim 2019;60:513–25.

[40] Yan Z, Mi X, Hao L, Liang G, Sheng C. Multiscale concurrent topology optimization for cellular structures with multiple microstructures based on ordered SIMP interpolation. Comput Mater Sci 2018;155:74–91.

[41] Xiao M, Liu X, Zhang Y, Gao L, Gao J, Chu S. Design of graded lattice sandwich structures by multiscale topology optimization. Comput Methods Appl Mech Engrg 2021;384:113949.

[42] Liu J, Zou Z, Gao K, Yang J, He S, Wu Z. A novel digital unit cell library generation framework for topology optimization of multi-morphology lattice structures. Compos Struct 2025;354:118824.

[43] Li Z, Chu S, Wu Z. A novel bio-inspired design method for porous structures: variable-periodic Voronoi tessellation. Mater Des 2024:113055.

[44] Sanders E, Pereira A, Paulino G. Optimal and continuous multilattice embedding. Sci Adv 2021;7(16):eabf4838.

[45] Do QT, Nguyen CHP, Choi Y. Homogenization-based optimum design of additively manufactured voronoi cellular structures. Addit Manuf 2021;45:102057.

[46] Lu H, Lee T-U, Ma J, Chen D, Xie YM. Designing 2D stochastic porous structures using topology optimisation. Compos Struct 2023;321:117305.

[47] Chen D, Gao K, Yang J, Zhang L. Functionally graded porous structures: Analyses, performances, and applications–A review. Thin-Walled Struct 2023;191:111046.

[48] Garner E, Wu J, Zadpoor AA. Multi-objective design optimization of 3D micro-architected implants. Comput Methods Appl Mech Engrg 2022;396:115102.

[49] Hong Y, Li X, Yan Z, Liu Z, Zhuang Z. Designing spongy-bone-like cellular materials: Matched topology and anisotropy. Int J Mech Sci 2025;285:109788.

[50] Senhora FV, Sanders ED, Paulino GH. Optimally-tailored spinodal architected materials for multiscale design and manufacturing. Adv Mater 2022;34(26):2109304.

[51] He Z, Wang G, Pindera M-J. Multiscale homogenization and localization of materials with hierarchical porous microstructures. Compos Struct 2019;222:110905.

[52] Altmann R, Henning P, Peterseim D. Numerical homogenization beyond scale separation. Acta Numer 2021;30:1–86.

[53] Feng F, Xiong S, Liu Z, Xian Z, Zhou Y, Kobayashi H, Kawamoto A, Nomura T, Zhu B. Cellular topology optimization on differentiable Voronoi diagrams. Internat J Numer Methods Engrg 2023;124(1):282–304.

[54] Hoffmann J, Donoughe S, Li K, Salcedo MK, Rycroft CH. A simple developmental model recapitulates complex insect wing venation patterns. Proc Natl Acad Sci 2018;115(40):9905–10.

[55] Lagae A, Dutré P. A comparison of methods for generating Poisson disk distributions. Comput Graph Forum 2008;27(1):114–29.

[56] Liu K, Tovar A. An efficient 3D topology optimization code written in Matlab. Struct Multidiscip Optim 2014;50:1175–96.

[57] Liu X, Gao L, Xiao M. An efficient multiscale topology optimization method for frequency response minimization of cellular composites. Eng Comput 2024;1–25.

[58] Ramírez-Gil FJ, Silva ECN, Montealegre-Rubio W. Design of topology-optimized functionally graded porous structures under transient loads. Int J Mech Sci 2024;284:109732.

[59] Gao T, Zhang W, Zhu J, Xu Y, Bassir DH. Topology optimization of heat conduction problem involving design-dependent heat load effect. Finite Elem Anal Des 2008;44(14):805–13.

[60] Schilder RJ, Marden JH. A hierarchical analysis of the scaling of force and power production by dragonfly flight motors. J Exp Biol 2004;207(5):767–76.

[61] Wakeling J, Ellington CP. Dragonfly flight: I. Gliding flight and steady-state aerodynamic forces. J Exp Biol 1997;200(3):543–56.

[62] Appel E, Heepe L, Lin C-P, Gorb SN. Ultrastructure of dragonfly wing veins: composite structure of fibrous material supplemented by resilin. J Anat 2015;227(4):561–82.

[63] Yang Z, Qiu H, Gao L, Cai X, Jiang C, Chen L. Surrogate-assisted classification-collaboration differential evolution for expensive constrained optimization problems. Inform Sci 2020;508:50–63.

[64] Zhou M, Cui M, Xu D, Zhu S, Zhao Z, Abusorrah A. Evolutionary optimization methods for high-dimensional expensive problems: A survey. IEEE/CAA J Autom Sin 2024;11(5):1092–105.

[65] Fujita Y, Iima M. Dynamic lift enhancement mechanism of dragonfly wing model by vortex-corrugation interaction. Phys Rev Fluids 2023;8(12):123101.

[66] Kesel AB. Aerodynamic characteristics of dragonfly wing sections compared with technical aerofoils. J Exp Biol 2000;203(20):3125–35.

[67] Rajabi H, Rezasefat M, Darvizeh A, Dirks J-H, Eshghi S, Shafiei A, Mostofi TM, Gorb SN. A comparative study of the effects of constructional elements on the mechanical behaviour of dragonfly wings. Appl Phys A 2016;122:1–13.

[68] Combes SA, Daniel T. Flexural stiffness in insect wings II. Spatial distribution and dynamic wing bending. J Exp Biol 2003;206(17):2989–97.

[69] Rajabi H, Moghadami M, Darvizeh A. Investigation of microstructure, natural frequencies and vibration modes of dragonfly wing. J Bionic Eng 2011;8(2):363–4.

[70] Chu S. Simultaneous sizing, layout and topology optimization for buckling and postbuckling of stiffened panels (Ph.D. thesis), Cardiff University; 2022.

[71] Rajabi H, Ghoroubi N, Stamm K, Appel E, Gorb S. Dragonfly wing nodus: a one-way hinge contributing to the asymmetric wing deformation. Acta Biomater 2017;60:330–8.

[72] Sun W, Wang L, Wang YQ. Wing–wing coupling enhances the aerodynamic performance of dragonflies during forward flight. Phys Fluids 2025;37(1).

[73] Shumway N, Gabryszuk M, Laurence S. The impact of dragonfly wing deformations on aerodynamic performance during forward flight. Bioinspiration Biomimetics 2020;15(2):026005.

[74] Bluman J, Kang C-k. Achieving hover equilibrium in free flight with a flexible flapping wing. J Fluids Struct 2017;75:117–39.

[75] Heathcote S, Gursul I. Flexible flapping airfoil propulsion at low Reynolds numbers. AIAA J 2007;45(5):1066–79.

[76] Kang C-K, Aono H, Cesnik CE, Shyy W. Effects of flexibility on the aerodynamic performance of flapping wings. J Fluid Mech 2011;689:32–74.

[77] Addo-Akoto R, Han J-S, Han J-H. Aerodynamic characteristics of flexible flapping wings depending on aspect ratio and slack angle. Phys Fluids 2022;34(5).

[78] Lucas KN, Thornycroft PJ, Gemmell BJ, Colin SP, Costello JH, Lauder GV. Effects of non-uniform stiffness on the swimming performance of a passively-flexing, fish-like foil model. Bioinspiration Biomimetics 2015;10(5):056019.

[79] Zhao L, Huang Q, Deng X, Sane SP. Aerodynamic effects of flexibility in flapping wings. J R Soc Interface 2010;7(44):485–97.

[80] Chitsaz N, Siddiqui K, Marian R, Chahl J. Numerical and experimental analysis of three-dimensional microcorrugated wing in gliding flight. J Fluids Eng 2022;144(1):011205.